Acoustic phonon confinement in silicon nanolayers: Effect on electron mobility

L. Donetti, F. Gámiz,[a] J. B. Roldán, and A. Godoy
Departamento de Electrónica y Tecnología de Computadores, Universidad de Granada, 18071 Granada, Spain

(Received 25 January 2006; accepted 18 April 2006; published online 6 July 2006)

We demonstrate the confinement of acoustic phonons in ultrathin silicon layers and study its effect on electron mobility. We develop a model for confined acoustic phonons in an ideal single-layer structure and in a more realistic three-layer structure. Phonon quantization is recovered, and the dispersion relations for distinct phonon modes are computed. This allows us to obtain the confined phonon scattering rates and, using Monte Carlo simulations, to compute the electron mobility in ultrathin silicon on insulator inversion layers. Thus, comparing the results with those obtained using the bulk phonon model, we are able to conclude that it is very important to include confined acoustic phonon models in the electron transport simulations of ultrathin devices, if we want to reproduce the actual behavior of electron transport in silicon layers of nanometric thickness. © *2006 American Institute of Physics*. [DOI: 10.1063/1.2208849]

I. INTRODUCTION

Silicon-on-insulator (SOI) technology has been identified as the "vehicle" for achieving an increase in the operational speed of integrated circuits, which is necessary in order to extend the life of traditional silicon technology as we approach the end of the International Technology Roadmap for Semiconductors (ITRS).[1,2] A great deal of research effort has been devoted in the last few years to improving this technology in all fields: from materials and manufacturing techniques to circuits, and from devices to systems and end-user applications.[3] The advantages of SOI technology relate to the use of an insulating substrate, which reduces the number of steps in the device manufacturing process and also enables better control of the short channel effects. Transistors with gate lengths of 25 nm or less do not perform well in bulk Si. The electric field in the transistor channel induced by the gate has to compete with fields from the source and drain regions. These "short channel effects" (SCEs) are reduced or eliminated by using ultrathin SOI structures. There is close-to-unanimous agreement among experts in the field that ultrathin SOI is a key solution to the SCEs.[4,5] In addition, nowadays, SOI technology is sufficiently advanced to provide high-quality ultrathin SOI wafers with silicon layers of nanometric thicknesses on an industrial scale.[6] However, some drawbacks have already been pointed out: a serious mobility degradation in Si ultrathin body (UTB) metal-oxide-semicondctor field effect transistor (MOSFETs) with silicon thickness d_{Si} smaller than 5 nm has been reported in a recent experiment;[7] this could seriously limit the attainment of SOI goals.

It is well known that electron transport in ultrathin silicon layers is greatly modified from that in bulk silicon inversion layers. This modification is basically due to three principal phenomena. Firstly, the reduction in electron momentum dimensionality and the momentum and energy conservation laws produce a dramatic increase in the phonon scattering rate as the silicon thickness decreases.[8] Secondly, redistribution of the carriers among the different subbands due to quantum effects produces a decrease in the average conduction effective mass and therefore a mobility increase.[8] The third phenomenon arises due to modifications of the phonon modes caused by acoustic and dielectric mismatches between the silicon and the silicon dioxide. These changes in properties give rise to confined and interface phonons in quantum wells, quantum wires, and quantum dots.[9] The first two phenomena—increase in the phonon scattering rate and decrease in the average conduction effective mass in ultrathin silicon-on-insulator inversion layers—have been previously studied elsewhere.[8,10] It was shown that electron mobility behavior in SOI devices is a complex function of the silicon thickness as a direct consequence of the superposition of two opposite effects.[8] With regard to the third phenomenon, confined acoustic phonons have recently been observed in experiments on very thin silicon layers.[9] Over the last few years, some theoretical work has also been developed in III-V based devices (see Refs. 11 and 12 and references therein). The electron-acoustic phonon scattering affects two important physical properties, namely, thermal conduction[13] and charge carrier mobility.[12] For this reason, modifications in the phonon spectrum are of strategic interest to device engineers and scientists. Up to now, this phonon confinement has been neglected in the calculation of electron mobility in ultrathin silicon inversion layers, and bulk phonon scattering models have been adopted.[8,14] In this work we provide proof of the importance of acoustic phonon confinement in electron mobility. We achieve this by calculating electron mobility curves in double gate silicon-on-insulator (DGSOI) devices for different values of d_{Si}, taking into account phonon confinement, and comparing the results to those obtained when phonon confinement is ignored.

The structure of this paper is as follows. First of all, following Refs. 11 and 12, we introduce an elastic continuum

[a]Electronic mail: fgamiz@ugr.es

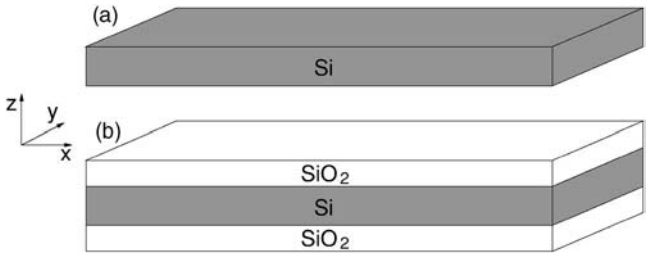

FIG. 1. Device structures considered for the acoustic phonon quantization study.

model for acoustic phonons in a simplified structure with only one silicon layer. Two different boundary conditions are considered: in (i) the external surfaces are rigid and fixed; in (ii) they are free. These boundary conditions give rise to phonon quantization: a discrete set of values is only allowed for the wave vector in the confined dimension. Dispersion relations are obtained for the different phonon branches and for different values of the silicon thickness. Using this phonon model, we obtain the electron scattering rate for a DG-SOI device at room temperature, and finally we compute the electron mobility using Monte Carlo simulations. These results are then compared to those obtained using the bulk model for acoustic phonons. Once the importance of phonon confinement has been verified, we consider a more realistic structure with two oxide layers enclosing the silicon one; we compute the dispersion relations, the electron scattering rates, and the electron mobility, and discuss how these results are affected by acoustic phonon confinement. Some conclusions are finally drawn.

II. ELASTIC CONTINUUM MODEL OF ACOUSTIC PHONONS

The confined phonon model is based on the elastic continuum model of acoustic phonons (see, for example, Ref. 11 for a detailed discussion): phonons are represented by elastic waves in a continuous medium. The equation for the displacement vector $\mathbf{u}$ in an isotropic medium can be written as

$$\frac{\partial^2 \mathbf{u}}{\partial t^2} = s_t^2 \nabla^2 \mathbf{u} + (s_l^2 - s_t^2)\, \nabla\, (\nabla \mathbf{u}), \tag{1}$$

where s_t and s_l are the transversal and longitudinal sound speeds, respectively.

We solve the above equation in the structures shown in Fig. 1 for different boundary conditions.

First of all, we consider a single silicon layer of thickness $d = d_{\mathrm{Si}}$ parallel to the xy plane [see Fig. 1(a)], and we look for normalized solutions of the form.[11]

$$\mathbf{u}(\mathbf{r}_\parallel, z) = \mathbf{w}_n(\mathbf{q}_\parallel, z) e^{i\mathbf{q}_\parallel \cdot \mathbf{r}_\parallel - i\omega_n t}, \tag{2}$$

where $\parallel$ denotes vector components in the xy plane, which is the plane parallel to the $\mathrm{Si}-\mathrm{SiO_2}$ interfaces. If we consider the boundary surfaces as rigid and fixed, the displacement vector must vanish on the external surfaces, i.e., $\mathbf{u}=0$ for $z = \pm d/2$; another possible type of boundary condition is the free-standing one, where the z components of the stress tensor (T_{xz}, T_{yz}, T_{zz}) vanish.

The usual quantization rules yield the representation of the displacement $\mathbf{u}$ in terms of phonons:

$$\mathbf{u} = \sum_{\mathbf{q}_\parallel, n} \sqrt{\frac{\hbar}{2A\rho\omega_n}} [a_n(\mathbf{q}_\parallel) + a_n^\dagger(-\mathbf{q}_\parallel)] \mathbf{w}_n(\mathbf{q}_\parallel, z) e^{i\mathbf{q}_\parallel \cdot \mathbf{r}_\parallel - i\omega_n t}, \tag{3}$$

where a_n and $a_n^\dagger$ are the creation and annihilation operators of phonons, A denotes the area of the layer in the xy plane, and ρ is the material density. The interaction Hamiltonian then reads

$$H_{\mathrm{int}} = D_{ac} \nabla \mathbf{u} = D_{ac} \sum_{\mathbf{q}_\parallel, n} \sqrt{\frac{\hbar}{2A\rho\omega_n}} [a_n(\mathbf{q}_\parallel) + a_n^\dagger(-\mathbf{q}_\parallel)] \Gamma(z) e^{i\mathbf{q}_\parallel \cdot \mathbf{r}_\parallel - i\omega_n t}, \tag{4}$$

where

$$\Gamma(z) = i\mathbf{q}_\parallel \cdot \mathbf{w}_n(\mathbf{q}_\parallel, z) + \frac{\partial w_{n,z}(\mathbf{q}_\parallel, z)}{\partial z}. \tag{5}$$

Without loss of generality we can assume that $\mathbf{q}_\parallel$ is directed along the x axis, that is, $\mathbf{q}_\parallel = (q, 0)$; the equations for the components of $\mathbf{w}$ follow:

$$\begin{aligned} -\omega^2 w_x(z) &= \left(s_t^2 \frac{d^2}{dz^2} - s_l^2 q^2\right) w_x(z) + i(s_l^2 - s_t^2) q \frac{d}{dz} w_z(z), \\ -\omega^2 w_y(z) &= s_t^2 \left(\frac{d^2}{dz^2} - q^2\right) w_y(z), \\ -\omega^2 w_z(z) &= \left(s_l^2 \frac{d^2}{dz^2} - s_t^2 q^2\right) w_z(z) + i(s_l^2 - s_t^2) q \frac{d}{dz} w_x(z). \end{aligned} \tag{6}$$

The y component is decoupled from the others, giving solutions where the only nonzero component is w_y; these are known as shear waves. The x and z components, however, are coupled and, due to the symmetry of the system with respect to the xy plane, we can have solutions with a symmetric w_x and an antisymmetric w_z (dilatational waves) or solutions with an antisymmetric w_x and a symmetric w_z (flexural waves).

Starting with the case of rigid surface boundary conditions,[15] the shear wave solutions for the boundary conditions $w_y(\pm d/2) = 0$ are calculated easily as

$$w_y(z) = \begin{cases} N \cos\left(\dfrac{n\pi}{d} z\right), & n = 1,3,5,\ldots \\ N \sin\left(\dfrac{n\pi}{d} z\right), & n = 2,4,6,\ldots, \end{cases} \tag{7}$$

with

$$\omega = s_t \sqrt{q^2 + \left(\frac{n\pi}{d}\right)^2}. \tag{8}$$

These phonons do not interact with electrons because $\Gamma(z) = 0$, according to Eq. (5).

The dilatational wave general solution corresponds to a linear superposition of two terms:

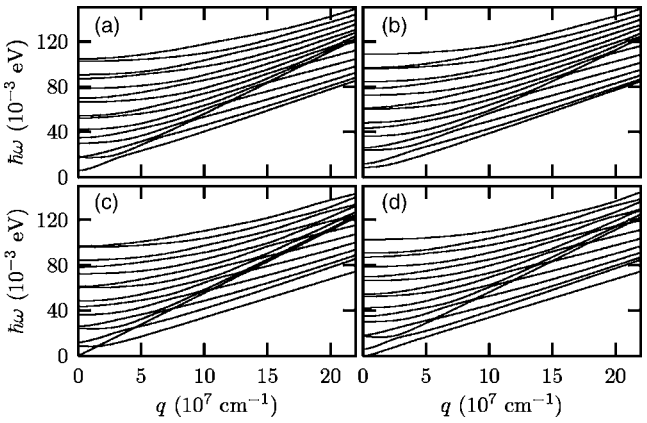

FIG. 2. Branches of the dispersion relation for a 2 nm Si layer; (a) and (b) are the dilatational and flexural waves for rigid surface boundary conditions, (c) and (d) the same for free boundary conditions.

$$w_x(z) = iAq\cos(q_l z) + iBq_t\cos(q_t z),$$
$$w_z(z) = -Aq_l\sin(q_l z) + Bq\sin(q_t z), \tag{9}$$

with frequency ω given by

$$\omega^2 = s_l^2(q^2+q_l^2) = s_t^2(q^2+q_t^2). \tag{10}$$

The interaction function $\Gamma(z)$ then reads

$$\Gamma(z) = -A(q^2+q_l^2)\cos(q_l z). \tag{11}$$

By imposing the boundary conditions $w_x(\pm d/2)=0$ and $w_z(\pm d/2)=0$ we obtain a linear homogeneous system of two equations with two unknowns A and B; a nonzero solution only exists if the determinant of the corresponding matrix vanishes, that is,

$$q^2\tan(q_t d/2) + q_l q_t\tan(q_l d/2) = 0, \tag{12}$$

where q_l and q_t are functions of the frequency ω obtained by Eq. (10). In this way, we obtain a discrete set of permitted frequencies for each value of q describing the quantized phonon modes.

Similarly, the general solution for the flexural case is given by

$$w_x(z) = iAq\sin(q_l z) + iBq_t\sin(q_t z),$$
$$w_z(z) = Aq_l\cos(q_l z) - Bq\cos(q_t z), \tag{13}$$

and the interaction is

$$\Gamma(z) = -A(q^2+q_l^2)\sin(q_l z). \tag{14}$$

The existence of solutions satisfying the boundary conditions requires

$$q^2\tan(q_l d/2) + q_l q_t\tan(q_t d/2) = 0. \tag{15}$$

The resulting dispersion relations for a 2 nm silicon layer ($s_l = 8.43\times10^5$ cm/s, $s_t = 5.84\times10^5$ cm/s) are shown in Figs. 2(a) and 2(b). There are different branches corresponding to the different solutions of Eqs. (12) and (15) for the same value of q. All branches are "optical-like:" the frequency is nonzero even for $q\to0$. Each curve starts as a slowly varying function for small values of q; then all proceed to bend in a complex way, the only clear feature being that their superposition almost reproduces the longitudinal bulk dispersion line $\omega = s_l q$. For larger values of q their slopes decrease, and the curves asymptotically approach the transversal bulklike dispersion relation $\omega = s_t q$.

Let us now turn to the free-standing boundary conditions.[11,16] In the case of shear waves, when the only nonzero component is w_y, the components T_{xz} and T_{zz} of the stress tensor vanish, while

$$T_{yz} = \rho s_t^2\frac{dw_y}{dz}. \tag{16}$$

To satisfy the boundary condition, the derivative of $w_y(z)$ must vanish at $z=\pm d/2$, producing the following solutions:

$$w_y(z) = \begin{cases} N\sin\left(\dfrac{n\pi}{d}z\right), & n = 1,3,5,\ldots \\ N\cos\left(\dfrac{n\pi}{d}z\right), & n = 0,2,4,\ldots, \end{cases} \tag{17}$$

with the same dispersion relation (8) as in the case of rigid surface boundary conditions. As before, interaction with electrons vanishes; i.e., $\Gamma(z)=0$.

For dilatational and flexural waves, the nonzero components of the displacement vector are w_x and w_z; the T_{yz} component of the stress tensor vanishes, while we have

$$T_{xz} = \rho s_t^2\left(\frac{dw_x}{dz} + iqw_z\right),$$
$$T_{zz} = \rho\left[s_l^2\frac{dw_z}{dz} + iq(s_l^2-2s_t^2)w_x\right]. \tag{18}$$

The general solutions are the same as before [Eqs. (9) and (13)] and, imposing the boundary conditions $T_{yz}(\pm d/2) = T_{zz}(\pm d/2) = 0$, we obtain

$$4q^2 q_l q_t\tan(q_l d/2) + (q^2-q_t^2)^2\tan(q_t d/2) = 0 \tag{19}$$

for the dilatational waves, and

$$4q^2 q_l q_t\tan(q_t d/2) + (q^2-q_t^2)^2\tan(q_l d/2) = 0 \tag{20}$$

for the flexural waves.

The corresponding dispersion branches for the same structure as before are shown in Figs. 2(c) and 2(d). Now there is one "acousticlike" branch, for which $\omega\to0$ as $q\to0$; those remaining are qualitatively similar to the ones in the previous case, showing the same asymptotic behavior.

III. SCATTERING RATE AND ELECTRON MOBILITY

Once the dispersion relations for the phonons in thin layers have been computed, we can evaluate the interaction Hamiltonian using Eqs. (4) and (5) and then compute the scattering rates. These are computed using the *Fermi golden rule*, which gives the transition probability density between two states i and f:[17]

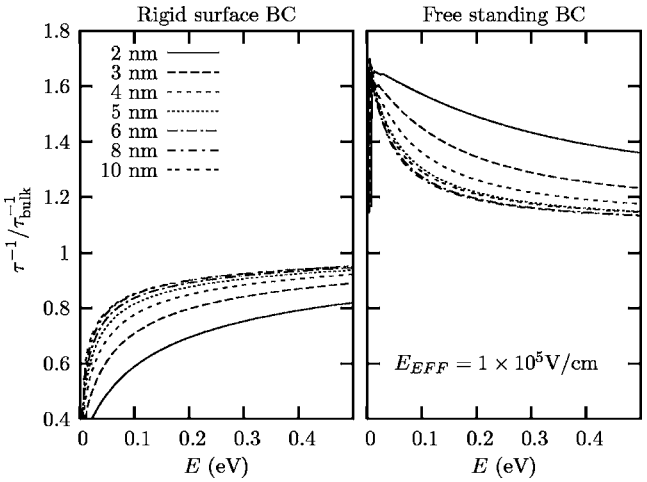

FIG. 3. Confined acoustic phonon scattering rate normalized to the bulk elastic scattering rate, as a function of initial electron energy, for different silicon layer thicknesses.

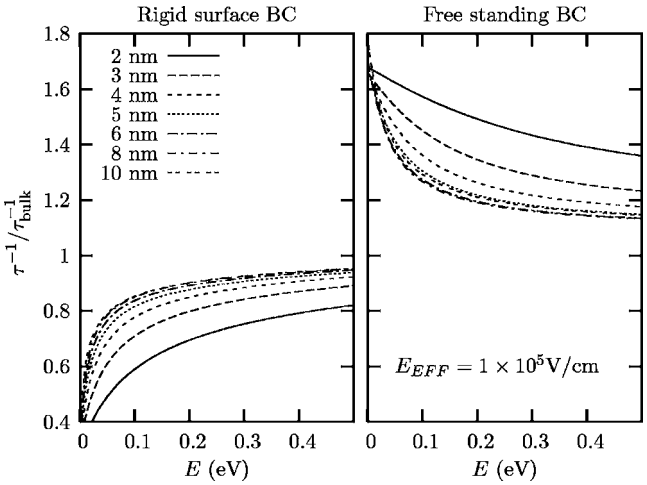

FIG. 4. Confined acoustic phonon scattering rate in elastic approximation normalized to the bulk elastic scattering rate, as a function of initial electron energy, for different silicon layer thicknesses.

$$W_{i\to f} = \frac{2\pi}{\hbar}|\langle f|H_{\text{int}}|i\rangle|^2 \delta(\epsilon_f - \epsilon_i), \tag{21}$$

where the initial and the final states contain both the electron and the phonon states. The scattering rate is then obtained by integrating over the final state of the electron, taking into account the contributions of phonon absorption or emission, of different phonon types (dilatational or flexural) and phonon dispersion branches.[16]

Figure 3 shows the ratio of the scattering rate to that obtained using a bulk model with elastic approximation[18,19] as a function of the initial electron energy, for different layer thicknesses in a DGSOI device. Note that it shows only the intrasubband scattering rate for an electron in the first subband. The device is considered to be at room temperature (300 K); in this condition the main scattering mechanism is phonon scattering. As expected, fixed (rigid surface) boundary conditions limit the number of permitted vibrational modes and therefore produce a decrease in the scattering rate. This effect is intensified as the layer becomes thinner. Free boundary conditions, on the other hand, imply a larger number of available phonon modes. This fact produces an increase in the scattering rate, which grows as the silicon layer becomes thinner.

We then evaluate electron mobility as a function of silicon thickness in a double gate SOI MOSFET using a Monte Carlo simulator (described in Ref. 8). At this stage, only phonon scattering is taken into account to avoid any possible masking effect from other scattering mechanisms. Intervalley optical phonons are taken into account, assuming the usual bulk model, since optical phonon modes are not significantly affected by spatial confinement.[20] Using the exact scattering rates obtained with this model in the Monte Carlo simulations would be extremely costly from a computational point of view. Since the phonon energy is typically much smaller than the electron thermal energy at room temperature, we adopt an elastic approximation (also used in the bulk models) which speeds up the computation considerably: the electron energy is assumed not to change during an acoustic phonon scattering event. In Fig. 4 we plot the electron scattering rate computed in the elastic approximation: the comparison with Fig. 3 shows that the curves are almost identical except for minor differences when the electron energy is so small that the phonon scattering rate cannot be neglected.

In Fig. 5 we plot the phonon-limited electron mobility obtained in simulations using the bulk model (solid line) and the confined model with the two different boundary conditions (dashed line for free boundary conditions and dash-dotted line for rigid boundary conditions). The following conclusions can be obtained from this figure.

(i) In all three cases the curves are similar in shape: this complex shape is produced by the superposition of the two opposite effects mentioned in the Introduction. As the silicon thickness decreases, on the one hand, the subband modulation produces a mobility increase due

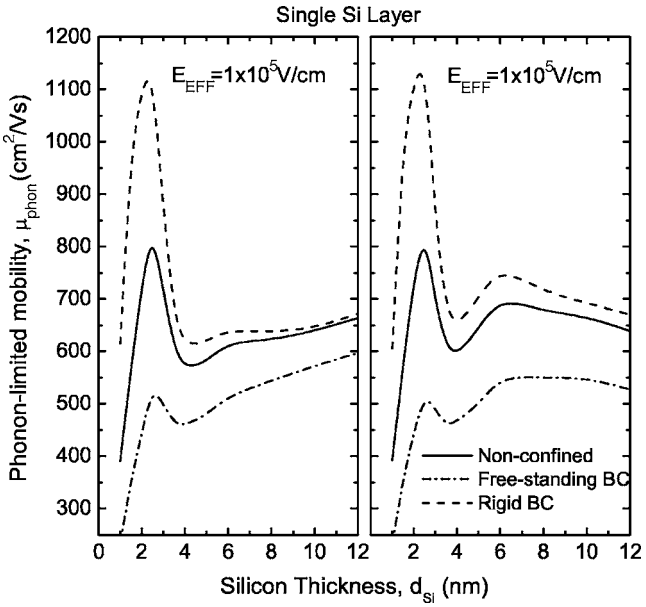

FIG. 5. Calculated electron mobility in double gate silicon-on-insulator inversion layers vs the silicon thickness for two values of the transverse effective field. Only phonon scattering has been taken into account, using a single-layer model for confined phonons.

to the lower conduction effective mass, and, on the other hand, the phonon scattering rate increases when phonons and electrons are more spatially confined.

(ii) For large silicon thicknesses, the mobility obtained with the confined phonon model approaches that of the bulk model.

(iii) When the silicon layer thickness is less than 5 nm, the differences with respect to the bulk model are very large: with rigid boundary conditions the mobility is greatly increased due to the fact that in this case the silicon vibrations are reduced and, consequently, the electron scattering rate decreases (as can be seen in Fig. 3). On the other hand, free boundary conditions increase the number of available phonon modes, which implies a larger scattering probability and, consequently, lower electron mobility.

The results obtained so far show that (i) it is possible to describe phonon quantization in thin layers and (ii) phonon quantization has a strong influence on electron mobility. However, in real SOI devices the silicon slab is enclosed between different materials (oxide, polysilicon, etc.). Therefore the actual boundary conditions are different from the two ideal boundary conditions previously considered. In the usual case for SOI devices, the silicon layer is enclosed between two oxide (SiO_2) layers. We would expect the properties of the device to lie somewhere between the two cases analyzed, rather closer to the free-standing case because the oxide sound speed is smaller than the silicon sound speed. However, to make quantitative predictions we need to develop a more realistic model.

IV. THREE-LAYER STRUCTURE

We now improve the model by considering the two SiO_2 layers which enclose the silicon layer [Fig. 1(b)]. Firstly, to preserve the symmetry of the system, we consider two layers of silicon dioxide of equal thickness d_{ox} around a silicon layer of thickness d_{Si}; later we will consider how to deal with oxide layers of unequal thicknesses. The equations are the same as before and again, the symmetry of the system allows us to classify the solutions as those with only nonzero y components (shear waves), those with symmetric x and antisymmetric z components (SA waves), and those with antisymmetric x and symmetric z components (AS waves). The shear waves still have a vanishing interaction Hamiltonian, and we will not consider them in detail. The SA (AS) waves consist of dilatational (flexural) waves in the silicon layer and a linear combination of all four waves [given by Eqs. (9) and (13)] in the two oxide layers. The actual solution must fulfill continuity equations for w_x, w_z, T_{xz}, and T_{zz} at the interface between silicon and oxide, and must obey the boundary condition (free-standing or rigid) at the external surfaces. We obtain a system of six linear homogeneous equations with six unknowns (the coefficients of two components in the silicon and four in the oxide); the dispersion relations are given by setting to zero the determinant of the matrix of the corresponding system.

If the two oxide layers have different thicknesses, the system loses its symmetrical properties. There are still shear waves that do not interact with electrons, but the distinction between waves with symmetric and with antisymmetric x and z components disappears. The solutions with nonzero w_x and w_z are now provided by the superposition of four components in each layer, giving a total of 12 coefficients to be determined. The solution must then fulfill continuity equations on the two silicon-oxide interfaces and boundary conditions on the external surfaces, with a total of 12 equations. Again, the dispersion relations are obtained by setting to zero the determinant of the corresponding system of equations.

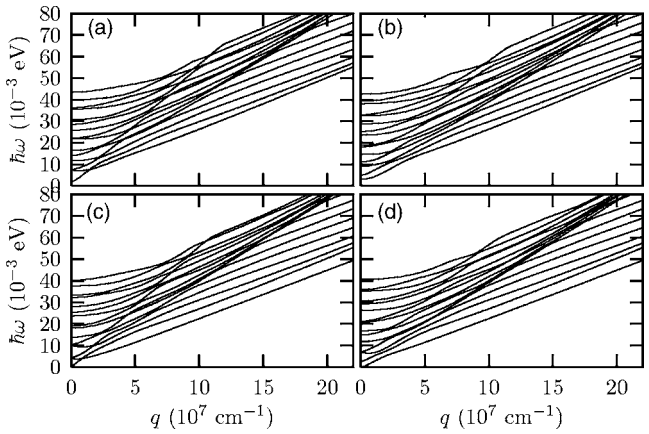

FIG. 6. Branches of the dispersion relation; (a) and (b) are the SA and AS waves for the rigid surface boundary conditions, (c) and (d) the same for free boundary conditions. The oxide thickness d_{ox} is 1 nm.

Figure 6 shows the dispersion branches for a symmetric structure with $d_{Si}=2$ nm and $d_{ox}=1$ nm ($s_l=5.97\times10^5$ cm/s, $s_t=3.77\times10^5$ cm/s for the silicon dioxide). The comparison between Figs. 6 and 2 shows two main differences between the dispersion relations in the two cases. First of all, the energy difference between the branches is typically much smaller when the oxide layers are considered; secondly, in this case the asymptotic slope of all branches is given by the transversal sound speed in the oxide, which is smaller than that in the silicon. These differences, however, do not give any insight into how the electron transport properties will be affected.

The electron scattering rate for the interaction with the confined phonons is then computed in the same way as in the single layer case. Figure 7 shows the ratio between the computed scattering rate and the rate obtained with the bulk model. In this case the scattering rate increases with both free and rigid boundary conditions; the difference grows as the silicon layer thickness decreases. In both cases the increase in the scattering rate is much lower than that found for a single silicon layer with free boundary conditions; for rigid boundary conditions, in fact, the scattering rate is close to that obtained with the bulk model when the silicon thickness approaches 10 nm.

As before, we use these scattering probabilities in the Monte Carlo simulator to evaluate electron mobility. In Fig. 8 we plot the phonon-limited electron mobility obtained for a DGSOI at room temperature. A significant reduction in mobility is observed when the confined phonon model is considered, regardless of the boundary condition set, the effect being greater for free-standing boundary conditions. The

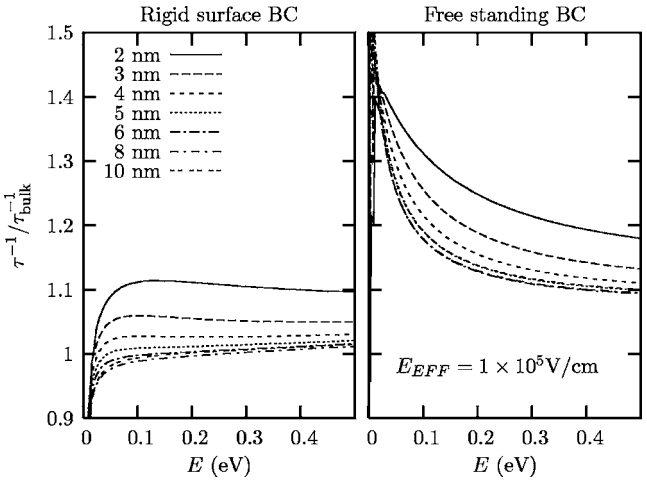

FIG. 7. Confined acoustic phonon scattering rate normalized to the bulk elastic scattering rate, as a function of initial electron energy, for different silicon layer thicknesses. The oxide thickness used for this calculation is 1 nm.

most significant corrections (which could rise to almost 30%) correspond to silicon thicknesses in the range of 5–10 nm, while previous results obtained with a bulk acoustic phonon model showed a considerable mobility increase due to the volume inversion effect.[8]

In real devices, phonon scattering is not the only mechanism to reduce electron mobility; when other mechanisms are taken into account, the effect of phonon confinement is reduced. For this reason we then include surface roughness scattering in the simulations to check that phonon confinement is still relevant. Note that Coulomb scattering is not taken into account because in ultrathin SOI devices the silicon layer could maintain its undoped state while SCEs remain under control.[2] Figure 9 shows the electron mobility obtained by the simulation if we include electron scattering

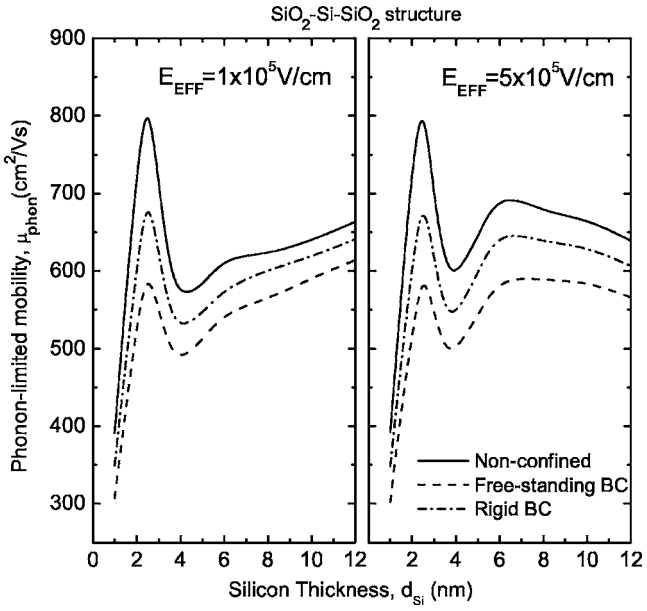

FIG. 8. Calculated electron mobility in double gate silicon-on-insulator inversion layers vs the silicon thickness for two values of the transverse effective field. Only phonon scattering was taken into account in this calculation.

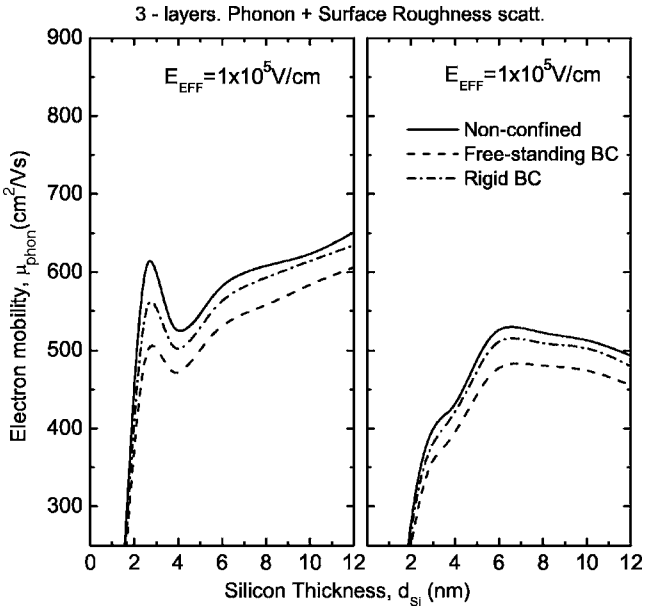

FIG. 9. Calculated electron mobility in double gate silicon-on-insulator inversion layers vs silicon thickness; surface roughness scattering has now been taken into account in addition to phonon scattering.

by the surface roughness of both interfaces.[21,22] In this case the mobility is greatly reduced and the effect of phonon confinement is clearly masked. However, especially at low field values, the confinement still affects mobility in a clearly observable manner.

Even this improved model is not completely realistic because the boundary conditions we have imposed do not reproduce the actual boundary conditions of the oxide-silicon-oxide structure. This is in fact surrounded by different materials, depending on the actual device under consideration [single gate, double gate, FIN Field Effect Transistor (FINFET) (Ref. 2)] or the gate material (polysilicon or metal). Therefore, in different cases the situation will more closely resemble either free or rigid boundary conditions. However, these two cases are extreme, and all possibilities should fall between the two shown here.

V. CONCLUSIONS

In conclusion, we have developed a model to describe the quantization of acoustic phonon modes due to spatial confinement in silicon nanolayers using different structures and different boundary conditions. Phonon quantization is recovered and the dispersion relations for distinct phonon modes are computed. This allows us to obtain the confined phonon scattering rates and to compute, using Monte Carlo simulations, the electron mobility in ultrathin silicon on insulator inversion layers. We have then shown that it is important to take into account acoustic phonon confinement in ultrathin silicon-on-insulator inversion layers by comparing electron mobility in ultrathin DGSOI devices, calculated assuming the usual bulk acoustic phonon model and also using the confined acoustic phonon model. Significant mobility reductions are obtained when the confined acoustic phonon model is used, even when other scattering mechanisms (such as surface roughness scattering) are taken into account. It is

therefore essential to include such a model in the electron transport simulations of ultrathin SOI devices if we want to reproduce the actual behavior of electrons in silicon layers of nanometric thickness.

ACKNOWLEDGMENTS

This work was partially carried out within the framework of Research Project Nos. FIS2005-06832 and TEC-2005-01948 supported by the Spanish Government and by the EU (Network of Excellence SINANO, IST-1-506844-NoE).

[1]http://public.itrs.net
[2]G. C. Celler and S. Cristoloveanu, J. Appl. Phys. **93**, 4955 (2003).
[3]http://www.eurosoi.org
[4]A. Vandooren, D. Jovanovic, S. Egley, M. Sadd, B.-Y. Nguyen, B. White, M. Orlowski, and J. Mogab, *2002 IEEE International SOI Conference, Williamsburg* (IEEE, Piscataway, NJ, 2002), p. 25.
[5]J. G. Fossum, V. P. Trivedi, and K. Wu, *2002 IEEE International SOI Conference, Williamsburg* (IEEE, Piscataway, NJ, 2002), p. 135.
[6]http://www.soitec.com/en/products/p_1.htm
[7]K. Uchida and S. Takagi, Appl. Phys. Lett. **82**, 2916 (2003).
[8]F. Gámiz and M. V. Fischetti, J. Appl. Phys. **89**, 5478 (2001).
[9]C. M. Sotomayor Torres, A. Zwick, F. Poinsotte, J. Groenen, M. Prunilla, J. Ahopelto, A. Mlayah, and V. Paillard, Phys. Status Solidi C **1**, 2609 (2004).
[10]F. Gámiz, J. B. Roldán, P. Cartujo-Cassinello, J. E. Carceller, J. A. López-Villanueva, and S. Rodríguez, J. Appl. Phys. **86**, 6269 (1999).
[11]N. Bannov, V. Mitin, and M. Stroscio, Phys. Status Solidi B **183**, 131 (1994).
[12]E. P. Pokatilova, D. L. Nikaa, and A. A. Balandin, Superlattices Microstruct. **33**, 155 (2003).
[13]M. Asheghi, Y. K. Leung, S. S. Wong, and K. E. Goodson, Appl. Phys. Lett. **71**, 1798 (1997).
[14]D. Esseni, M. Mastrapasqua, G. K. Celler, C. Fiegna, L. Selmi, and E. Sangiorgi. IEEE Trans. Electron Devices **48**, 2842 (2001).
[15]B. A. Glavin, V. I. Pipa, V. V. Mitin, and M. A. Stroscio, Phys. Rev. B **65**, 205315 (2002).
[16]N. Bannov, V. Aristov, V. Mitin, and M. A. Stroscio, Phys. Rev. B **51**, 9930 (1995).
[17]M. Lundstrom, *Fundamentals of Carrier Transport* (Cambridge University Press, 2000).
[18]P. J. Price, Ann. Phys. (N.Y.) **133**, 217 (1981).
[19]C. Jungemann, A. Emunds, and W. L. Engl, Solid-State Electron. **36**, 1529 (1993).
[20]A. Balandin and K. L. Wang, Phys. Rev. B **58**, 1544–1549 (1998).
[21]F. Gámiz, J. B. Roldán, J. A. López-Villanueva, P. Cartujo-Cassinello, and J. E. Carceller, J. Appl. Phys. **86**, 6854 (1999).
[22]F. Gámiz, J. B. Roldán, P. Cartujo-Cassinello, J. A. López-Villanueva, and P. Cartujo, J. Appl. Phys. **89**, 1764 (2001).